Stagnation-Point Ablation of Carbonaceous Flat Disks—Part II: Experiment

Chul Park*
NASA Ames Research Center, Moffett Field, California

Six flat-disk models made of carbon-carbon and carbon-phenolic materials were launched in an argon-filled track-range facility to test ablation characteristics in a radiation-dominated, massive-blowing environment. The shock standoff distances deduced from the shadowgraphs agree with theoretical predictions during the earlier portion of the flight, while the wall temperatures determined by the image-converter photographs agree with predictions during the later portion. The measured surface recessions exceed the calculated values by about 60% for carbon-phenolic and 30% for carbon-carbon. The discrepancies are attributed to spallation. The measured char thicknesses agree with theoretical predictions.

Introduction

THIS is the second part of a two-part work which follows Ref. 1, and in which the ablative characteristics of carbonaceous heat-shield materials were studied under a radiation-dominated, massive-blowing environment. The heat-shield materials have been tested hitherto only in a convectively heated environment or in a laser-irradiated environment, neither of which leads to a massive-blowing condition. To produce a massive-blowing condition, six flat-disk models 5 cm in diameter, two made of carbon-carbon and four of carbon-phenolic materials, were launched in a track-range facility filled with argon. The characteristics of the radiation emanating from the inviscid region of the shock layer over the model (and falling on the outer edge of the ablation layer) are calculated in Ref. 2 for such an environment. In Part I of this work, theoretical techniques were developed to compute simultaneously the heat and mass transfer through the ablation layer and the material responses at the stagnation region of the models. Calculations were made for the six cases tested to predict surface recessions, surface temperature history, and, for the carbon-phenolic materials, the char thicknesses.

The techniques and the results of the experiment are described here and compared with the theoretical predictions of Part I. The experiment involved the routine instrumentation techniques of the track-range facility, i.e., model launch and recovery, laser shadowgraph for flow visualization, and head-on ima-con (image-converter) pyrometric photography, all of which are described in Refs. 3-5. The environments of the tests are described in Part I and Ref. 5. The raw test data are presented in Ref. 6.

Test Data

Models and Templates

The flat-disk test models (Fig. 1) had a diameter of 5.08 cm, and the edges were rounded to a radius of approximately 0.16 cm. A reference groove was made on each model as shown. The diameter of the model and the location, width, and depth of the groove were measured before the test to an accuracy better than 0.013 mm. The Lexan base, 6.35 cm in diameter, fits inside the four steel tracks of the track-range facility.[1]

A template was made to fit the pretest dimensions of each model (see Fig. 1). The dimensions of the template were accurate also to within 0.013 mm. The surface referred to as "zero recession line" in Fig. 1 made a tight contact with the disk surface before the launch. Because of surface ablation, the flight through the range produced a gap between the zero ablation line and the surface of the model. The gap was measured after the flight to determine the recession of the surface.

Multidimensional carbon-carbon (CC) composite, FM 5055G chop-molded carbon-phenolic (CMCP), and FM 5055A inverted-chevron (Dixie cup) carbon-phenolic (ICCP) were used as the test materials. The materials were oriented into the most favorable, that is, least ablating, directions. In the case of the ICCP, the direction of the carbon cloth intersected the centerline of the model at 20 deg as shown in Fig. 1. The spacings between the adjacent layers of the cloth are approximately 0.5 mm when measured at the disk surface. The spacings between the adjacent reinforcing graphitized rods for the carbon-carbon are approximately 2.2 mm in one direction and 2.4 mm in the other when measured at the disk surface. For the CMCP, the 1.2 cm^2 carbon cloth coupons are laid in parallel with the disk surface.

Shadowgraph Data

A typical shadowgraph is shown in Fig. 2a. It is interpreted as illustrated in Fig. 2b. As shown here, the (vertical) width of the field of view is about 70% of the model diameter. The disk surface appears elliptic in the photograph instead of a straight line because of a yaw of the model and misalignment of the optical axis of the shadowgraph system; for the case shown, the optical axis is about 6.7 deg off the true normal to the axis of the model. To determine the shock standoff distance, the complete ellipse representing the projection of the edge of the disk, shown dotted in Fig. 2b, is first constructed. The shock standoff distance is then measured from the center of the ellipse to the visible shock front.

The shock standoff distances determined by this procedure are shown in Figs. 3a and 3b. The possible errors introduced by the above procedure and the intrinsic reading errors are estimated to be about ±0.3 mm, as indicated by the error bar in Fig. 3a. In Refs. 1 and 2, shock standoff distance Δ is determined for a disk immersed in an inviscid flow of argon contaminated by air

$$\Delta/R_d = (\epsilon)^{1/2}\ (1+\epsilon) \tag{1}$$

where R_d is the disk radius and ϵ is the mean density ratio

$$\epsilon = \rho_\infty / \rho_s$$

where ρ_∞ is the freestream density and ρ_s is the average density in the shock layer along the stagnation streamline. The

---

Received May 28, 1982; revision received Jan. 3, 1983. This paper is declared a work of the U.S. Government and therefore is in the public domain.

*Research Scientist, Entry Technology Branch. Member AIAA.

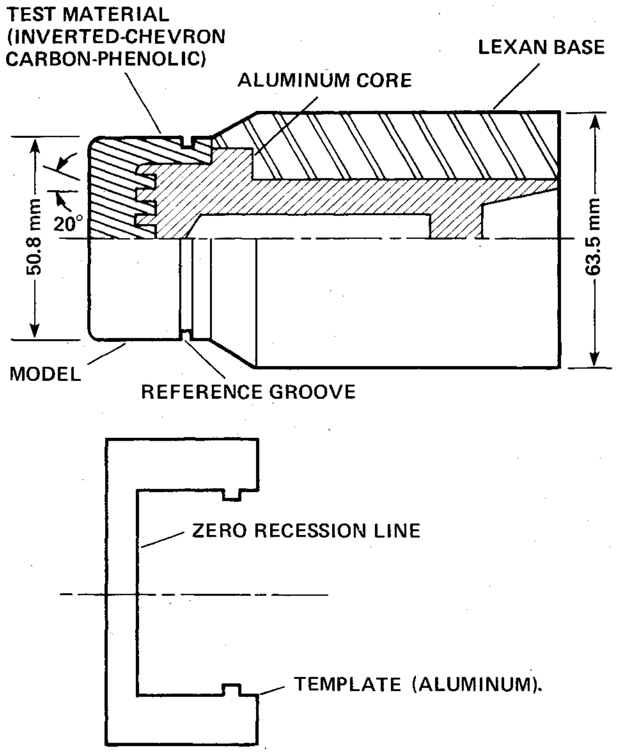

Fig. 1 Model and template.

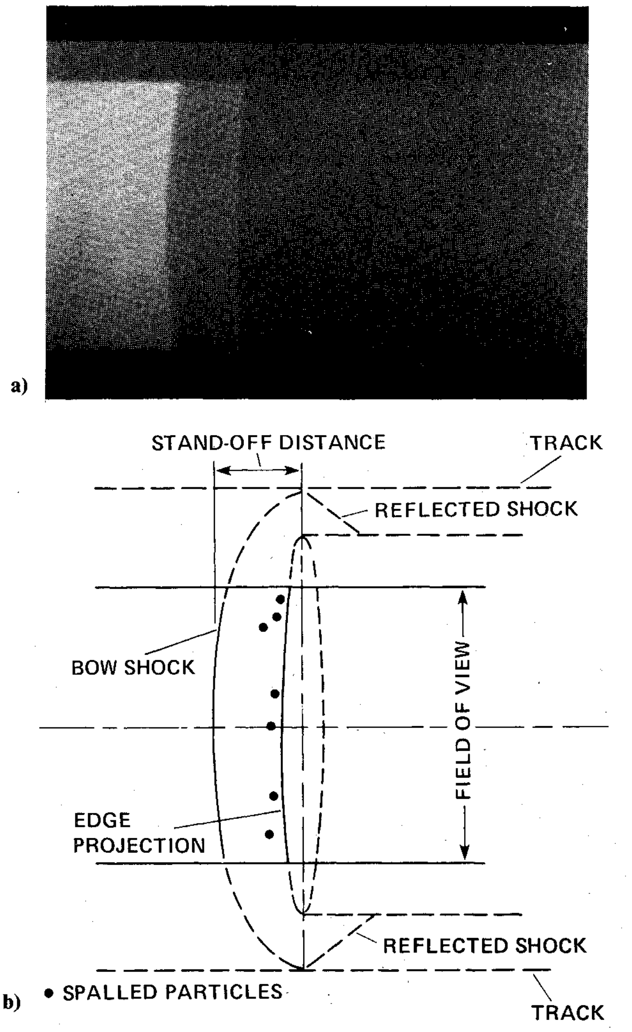

Fig. 2 Typical shadowgraph and its interpretation. Shot 5599 at $x = 182.3$ m.

calculated shock standoff distances are compared with the experimental values in Figs. 3a and 3b. In this comparison, boundary-layer thicknesses are neglected (Part I shows that the displacement thickness of the boundary layer is only about 0.5 mm).

Figures 3a and 3b show good agreement between the measured and predicted shock standoff distances in the first half of the model travel: the discrepancy between them is only about equal to or less than the estimated reading errors there. In the second half of the model travel, however, the measured standoff distances are consistently larger than the calculated values. This can be attributed to a severe yaw or pitch. Initially, the Lexan base fits tightly inside the tracks and pitch or yaw cannot develop to a significant extent. As the model travels inside the tracks, and the Lexan base wears because of friction, the fit becomes loose and pitch or yaw can develop. A weak trend of this kind is already seen in Figs. 2a and 2b: the major axis of the ellipse (projection of the rim of the disk) is not orthogonal to the axis of the track there. This trend worsens as the model travels. A small yaw or pitch can be accounted for by the procedure described above. When the yaw or pitch is large, however, the flow over the disk is no longer axisymmetric, and the shock standoff distance is not expected to be describable by Eq. (1). Taking this into account, the observed behavior of the shock standoff distance must be considered to be in reasonable agreement with the theoretical predictions. The general agreement between the theory and the experiment lends credence to the calculation method developed in Ref. 1.

Figures 2a and 2b also show what are interpreted to be spalled particles. There are nine such particles, which appear to be roughly spherical with diameters between about 0.2 and 0.7 mm for the case shown. In Table 1, the numbers of such particles are listed for all shots. The spalled particles are seen

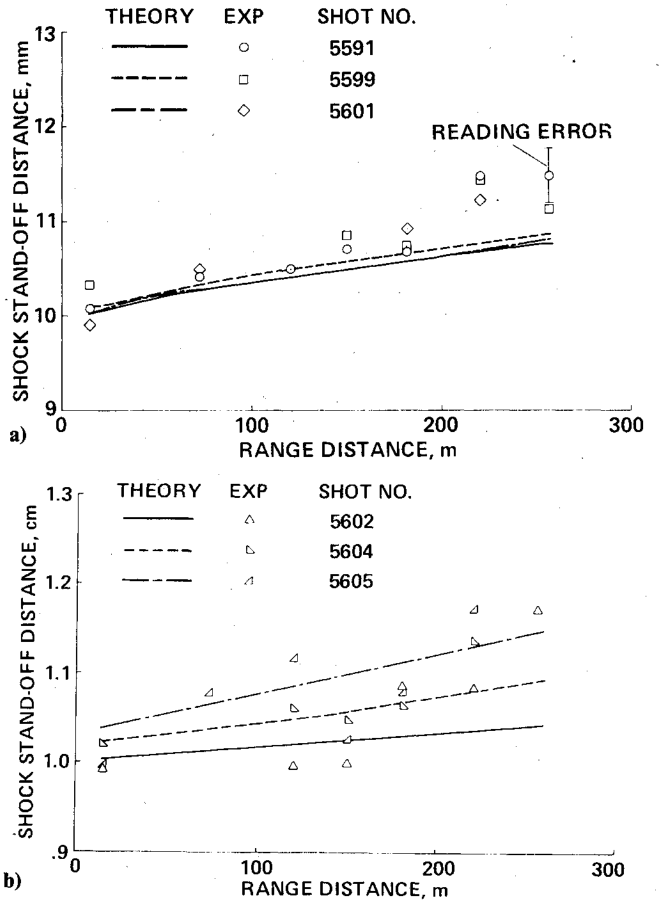

Fig. 3 Comparison of the measured and calculated shock standoff distances. a) Shots 5591, 5599, and 5601. b) Shots 5602, 5604, and 5605.

only for the CMCP, for which seven photographs out of a total of 17 exhibited the phenomenon. For shots 5599 and 5601, for which the stagnation pressures were between 25 and 32 atm,[1] the particles are found within approximately 20% of the standoff distance away from the disk wall. For shot 5602, for which the stagnation pressure was between 13 and 17 atm,[1] the particles are found at positions up to 40% of the shock standoff distance away from the wall.

Head-on Ima-Con Photographic Data

Figures 4a and 4b show typical examples of the head-on pyrometric image-converter photographs. In both figures, the images of the disk appear slightly asymmetric because the optical axes of the system are slightly off the true centerline axis of the track. Figure 4a shows an orthogonal pattern expected of the multidimensional CC composite material used, the dark spots being the ends of the reinforcing rods which are relatively cold because of the high thermal conductivity of the rods. The dark spots on the surface of the CMCP model (Fig. 4b) are attributed to indentation caused by the thermochemical ablation of the volatile resins or spallation.

Figure 4a shows a cloud of tiny bright spots outside the CC disk. These bright spots are attributed to the solid particles produced by spallation. For the two CC models tested, this phenomenon occurred rarely; in most photographs many fewer such spots are seen than are shown in Fig. 4a. The case shown in Fig. 4a is judged, therefore, to be a worst case of spallation. Figure 4b, the carbon-phenolic CMCP case, shows fewer but larger bright spots. These bright spots are attributed also to the spalled particles. For the four carbon-phenolic models tested, the bright spots were at least as prevalent as those seen in Fig. 4b. The case shown in Fig. 4b is interpreted, therefore, to be a weakly spalling case for carbon-phenolic.

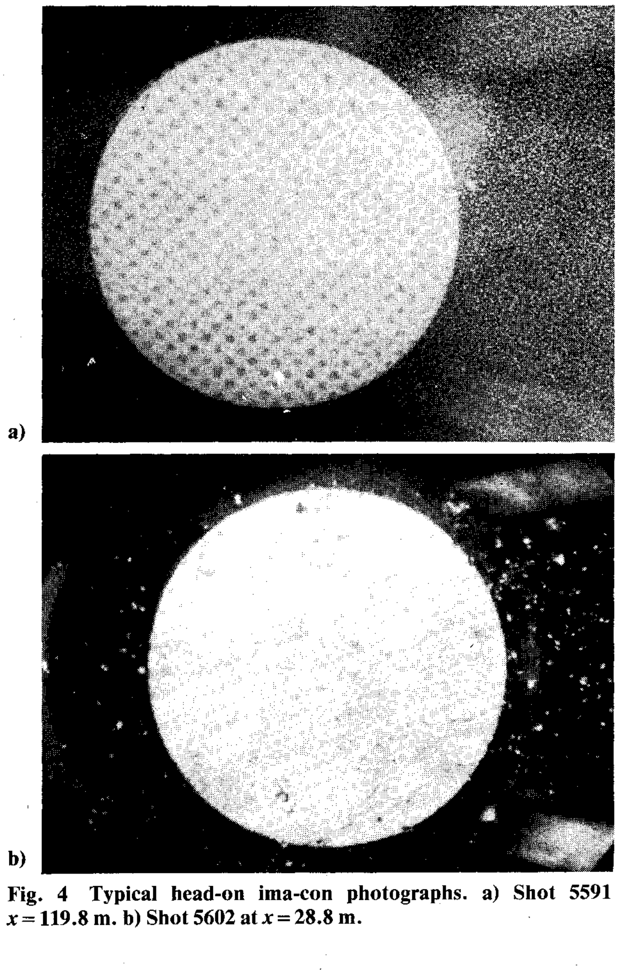

Fig. 4 Typical head-on ima-con photographs. a) Shot 5591 at $x = 119.8$ m. b) Shot 5602 at $x = 28.8$ m.

Figure 5 shows microphoto-densitometer traces of the photographs in Fig. 4. In both Figs. 5a and 5b, the scan direction was horizontal, that is, from left to right in Fig. 4. The abscissa in Fig. 5 is the scan distance, and the ordinate is temperature. The temperature scales are produced using the method described in Refs. 3 and 4, and are believed to be accurate to within a few hundred degrees. Figure 5a shows a temperature drop of about 100 K occurring at regular intervals corresponding to the spacings between the reinforcing rods; temperature drops on the surface of the carbon-phenolic models are irregular. Asymmetry of the temperature profiles is attributable to the finite inclination of the optical axis to the track centerline. Surface temperature increases slightly toward the edge of the disk in both Figs. 5a and 5b.

Finite temperatures of the regions outside the disks are attributed to the spalled particles. Luminosity of the spalled particles is relatively constant for the carbon-carbon model, but it is irregular for the carbon-phenolic model. The mean temperature of the cloud of the spalled particles is quite high when a massive spallation occurs: the difference between the temperature of the disk and the temperature of the cloud is less than 500 K for Fig. 5a. For the weakly spalling case (Fig.

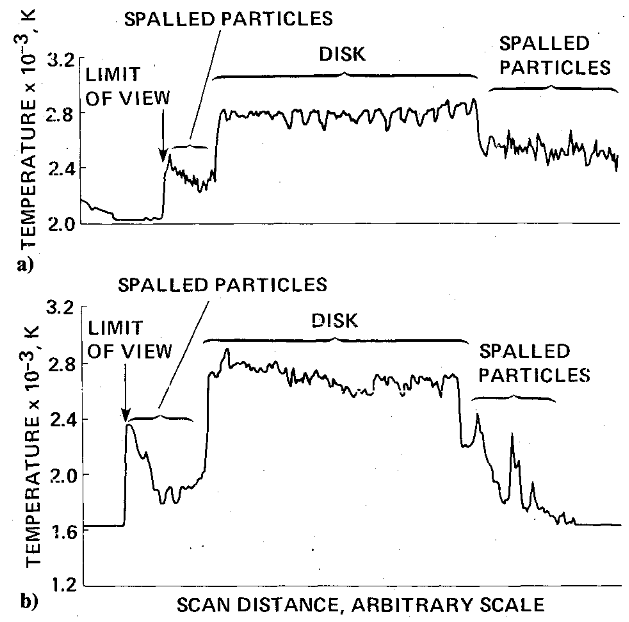

Fig. 5 Typical microphoto-densitometer traces of the head-on ima-con photographs. a) Shot 5591 at $x = 119.8$ m. b) Shot 5602 at $x = 28.8$ m.

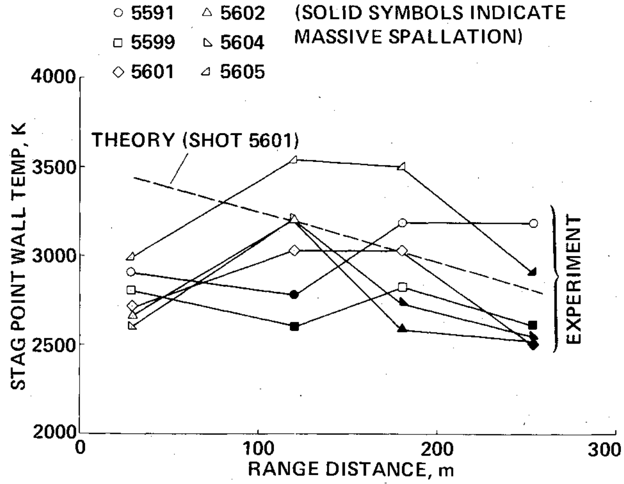

Fig. 6 Comparison of the measured and calculated stagnation-point temperatures.

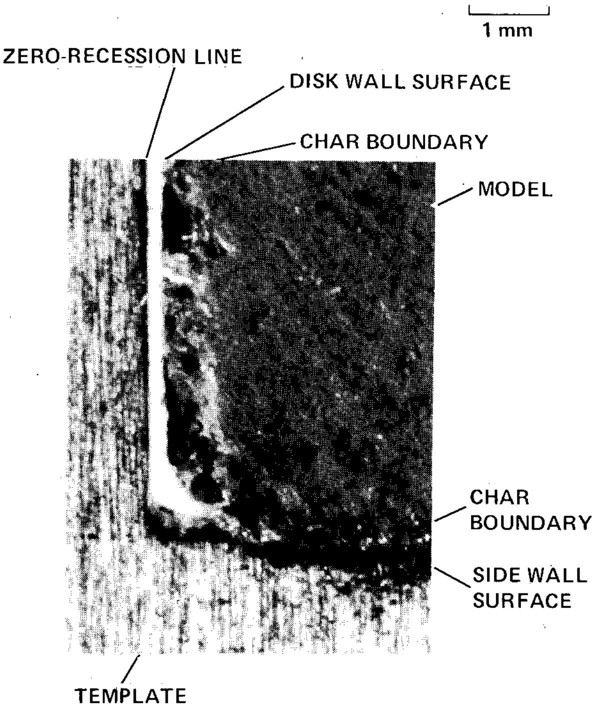

Fig. 7 Enlarged view of the cross section of a split model (shot 5601) mated to template.

Table 1 Number of visible spalled particles

Location	Shot No.					
x, m	5591 (CC)	5399 (CMCP)	5601 (CMCP)	5602 (CMCP)	5604 (ICCP)	5605 (CC)
16.1	0	0	0	0	0	0
73.5	0	–[a]	0	4	–	0
121.3	0	–	–	1	0	0
150.3	0	0	–	0	0	0
182.3	0	9	1	3	0	0
219.9	0	0	0	0	0	0
256.5	0	0	1	1	–	–

[a] Dash indicates photographic failures: too bright or too dim.

Table 2 Total indented areas for carbon-phenolic models

Shot No.	Material	Percent of disk surface area
5599	CMCP	3.8 ± 2
5601	CMCP	5.4 ± 1
5602	CMCP	4.2 ± 2
5604	ICCP	0.28 ± 0.05

5b), the difference is greater than 500 K. It thus becomes possible to quantitatively distinguish a massive spallation from a weak spallation: a massive spallation is a situation in which the mean temperature of the cloud of spalled particles differs from the surface temperature by less than 500 K. This characterization will be followed in the remainder of the paper.

In Fig. 6, the measured stagnation-point wall temperatures are plotted and are compared with the theoretical predictions of Part I. Both the theoretical and experimental wall temperatures are in the range 2500-3500 K. As described in Part I, these wall temperatures are reached while a model is passing through the helium environment in front of an ima-con camera. While a model is passing through argon, the wall temperatures are expected to be much higher. Because of the relatively low shock-layer temperatures in helium (about 3000 K), the model surfaces are cooled to temperatures approximately equal to the shock-layer temperatures. The occurrence of massive spallation is indicated by a solid symbol in the figure. Positions of the massive spallation, which occurs at least once for all shots, are unpredictable. The measured wall temperatures tend to be lower at stations where a massive spallation is observed. The theoretical values are shown for only one shot (shot 5601), because the theoretical wall temperatures are closely equal to the temperature of the helium shock layer.[1]

As seen in Fig. 6, the measured wall temperatures agree with the predicted values in the second half of the model travel. The predicted values pass through the approximate midpoints of the experimental data, and the difference between the theory and experiment is less than 500 K, the extent of possible experimental errors in temperature determination. In the first half of the model travel, however, the experimental data tend to be lower than the predicted values. The cause for this discrepancy is unknown, although it is speculated that the discrepancy can be attributed to spallation. Spallation has an effect of peeling the top layer of the material and exposing an inner surface. In the early part of a model travel, temperature decreases rapidly inward. Hence the exposed inner surface will be substantially cooler than the top surface. The evidence in support of this argument can be drawn from the fact that the measured wall temperatures are lower when a massive spallation occurs. Conversely, the high measured temperatures for some data points can be attributed to an equipment deficiency. If the valves controlling the flow of helium flushing argon in front of an ima-con camera fail to open at the precise instant, the model will pass through a mixture of argon and helium instead of pure helium, resulting in a higher shock-layer temperature. Taking these points into consideration, one can regard the behavior of the measured wall temperatures to be in reasonable agreement with the theoretical predictions.

The total area of the dark spots on the disk surface, which could be due to spallation, appearing in the last image-converter photograph ($x=253.3$ m) was measured for the four carbon-phenolic models. This was accomplished with the aid of a Hewlett-Packard Model HP 9864A digitizer connected to an HP 9830 computer. The measured spot areas are presented in Table 2 in terms of the percent of the disk surface area. As seen in the table, the three CMCP models have up to about 5% of their surface areas indented by what seems to be spallation; less than 0.5% of the surface areas of the ICCP models are similarly indented.

Cross-Sectional Data

The five recovered models were found to have diameters larger than those determined before the test. The diameters of the two carbon-carbon models were larger by about 0.08 mm on average, and those of the three carbon-phenolic models were larger by about 0.12 mm. In order to determine surface recessions and char thicknesses of the tested models, the models were sliced into two halves along a plane passing through the axis. The templates sketched in Fig. 1 were then fitted to each model. Photographs were taken of the cross sections of the models and the templates at an aperture of $f/45$. The special camera used for this purpose enlarged the image by a factor of 3.5 on the negative. The negatives are enlarged further by a factor of about 5.55 to produce positive prints, resulting in a 19.5-fold overall enlargement. This procedure resulted in large images of the cross sections without sacrificing the details.

Figure 7 shows one segment of such a photograph, in this case one corner of a carbon-phenolic model. One can see the changes in texture from the virgin carbon-phenolic to char. The zero recession line of the template (see Fig. 1), the recessed surface, the sidewall, and the virgin-to-char boundary are identified in the photograph. The char bound-

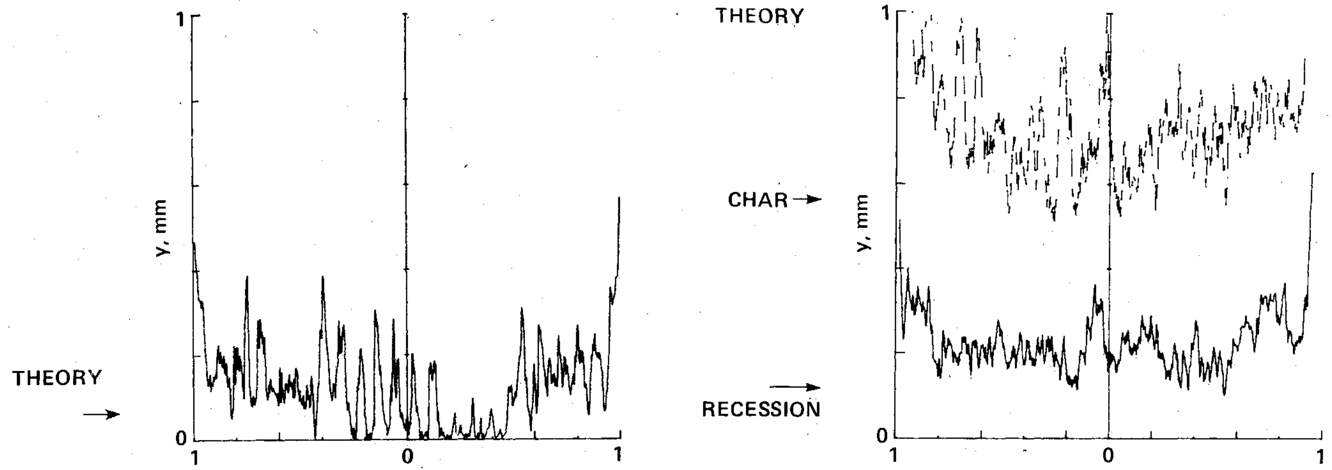

a) Shot 5591 (CC).

b) Shot 5599 (CMCP).

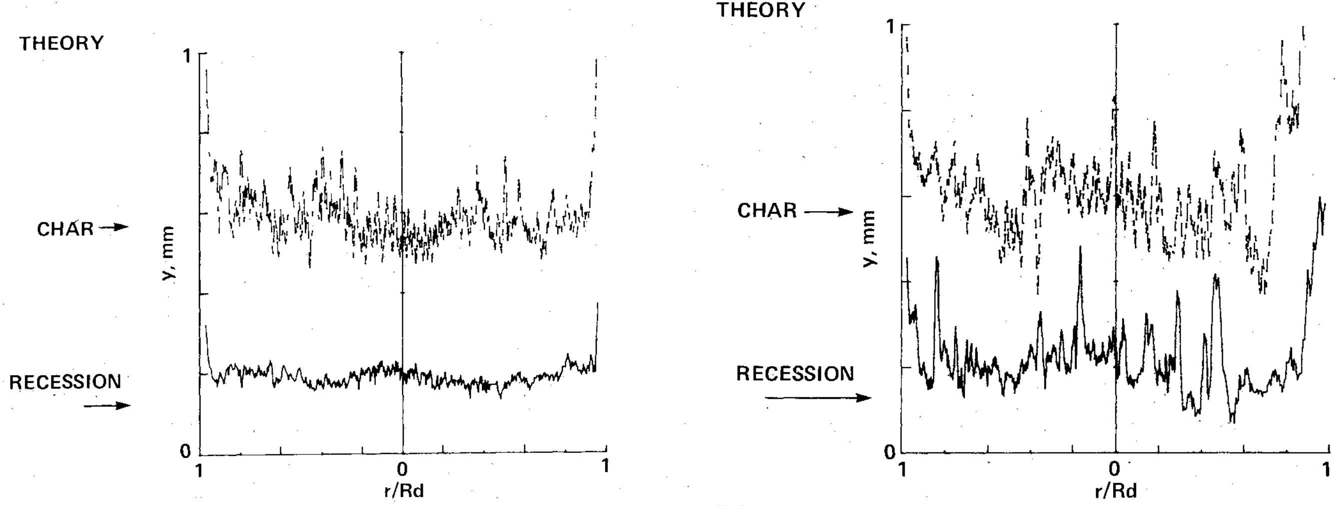

c) Shot 5601 (CMCP).

d) Shot 5604 (ICCP).

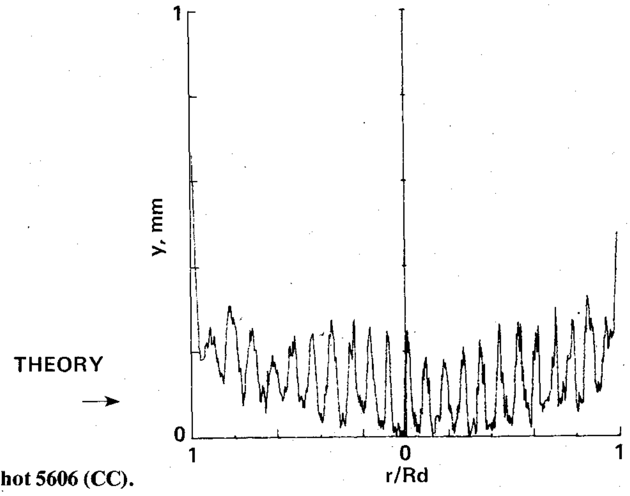

e) Shot 5606 (CC).

Fig. 8 Profile of wall surface (solid curve) and char boundary (dashed curve, for carbon-phenolic models only), compared with theoretical prediction of Ref. 1.

ary point is believed to be the point of maximum gradient in density change, which corresponds to the theoretical char boundary shown in Fig. 9 of Ref. 1. A deep indentation of the surface at one spot seen in the figure is typical of the carbon-phenolic models; it may be attributed to spallation.

The coordinates of the surface and the char boundary with respect to the zero recession line are determined at small intervals along radius *r* with the aid of a Hewlett-Packard Model HP 9864A digitizer. In Figs. 8a-e the measured wall-surface coordinates are shown as solid curves. For the carbon-phenolic models (shots 5599, 5601, and 5605; Figs. 8b-d), the char boundaries are shown as dashed curves in addition. The corresponding theoretical values for the stagnation point are shown by arrows on the left of the figures.

For the two carbon-carbon models (shots 5591 and 5605), the surfaces are indented at regular intervals. These intervals correspond to those of the dark spots in the head-on ima-con photographs in Fig. 4a, and to those of the cool spots in the microphoto-densitometer trace in Fig. 5a. The two CMCP models (Figs. 8b and 8c) show surfaces with irregular deep indentations. These indentations are the same kind as those seen in Fig. 7. In comparison, the ICCP model (Fig. 8d) has a much smoother surface. The relative frequencies of indentations seen in the three carbon-phenolic models roughly match the magnitude of the indented areas given in Table I.

The char boundaries of the two CMCP models are more irregular than those of the ICCP model. On the two CMCP models, however, the fluctuation in the boundary coordinates may be due partly to the uncertainty in the location of the boundary points; in many places the changes in texture take place far more gradually than was theoretically predicted (see Fig. 9 of Ref. 1).

Recessions on the carbon-phenolic models are larger than those on the carbon-carbon models. On the carbon-carbon models, the surface recession is minimal at about the stagnation point. For the carbon-phenolic models, however, the minimum recession occurs at a midpoint of the radius, i.e., about $r/R_d = 0.4$. On the two CMCP models (shots 5599 and 5601), the stagnation region shows more indentations than elsewhere.

In order to determine a true recession one must account for the swelling of the material. As mentioned earlier, the diameters of the models were increased during the flight through the test range. The cross-sectional photographs indicate that the thicknesses of the char under the sidewalls are approximately the same as those below the disk surfaces. Assuming that swelling is proportional to char thickness, the extent of swelling of the front surfaces is determined to be about 0.04 mm for the carbon-carbon and 0.06 mm for the carbon-phenolic models. These must be added to the surface coordinates to obtain the true recessions. Likewise, the true char thickness is the difference between the char boundary coordinate and the surface coordinate, minus the swell. To compare the theoretically predicted recessions with the experimental profiles in Figs. 8a-e, the swell must be subtracted from the theoretical values. The theoretical recession values so modified, and the theoretical coordinates of the char boundary which do not need correction, are shown in Figs. 8a-e alongside the experimental data. For the carbon-phenolic models, the theoretical predictions are made in Ref. 1 with two sets of thermal conductivity values for the material, one by Bueche of General Electric Co.,[7] which is referred to as the GE conductivities, and one by Wakefield and Pitts of Ames Research Center,[8] called Ames conductivities. The two sets of conductivity values are seen to yield nearly the same results.[1] The values obtained with the Ames conductivity values are shown in the figures.

To make the comparison more precise, average surface recessions were calculated regionally over an interval in r/R_d of 0.2 by integrating under the coordinates and dividing by the width of the integrating intervals. These regionally averaged recession values are averaged further over the left- and right-hand branches of the same profile, and over the different models of the same material. Figures 9 and 10 show the surface recessions and char thicknesses so averaged, and compare them with the corresponding theoretical average values. The absolute measured average recessions are 0.285 mm for the carbon-phenolic and 0.126 mm for the carbon-carbon models; the theoretical values are 0.176 (Ames conductivity) and 0.181 (GE conductivity) for carbon-phenolic and 0.0968 mm for carbon-carbon, respectively. The extent of the swells is shown also for comparison.

The error bars shown in the figures are the maximum extent of possible errors. They are arrived at by summing the following sources of errors: 1) errors in machining the templates = 0.025 mm; 2) errors introduced in reading of the photographs and digitizing = 0.005 mm; 3) errors in determining the extent of swelling = 0.013 mm; and 4) in determining char thicknesses, the errors in determining the char boundary points = 12% of the char thickness (see Fig. 7 of Ref. 1). Since the random errors decrease with the number of data points averaged, and since six and four data sets are used in averaging the carbon-phenolic and carbon-carbon data, respectively, the actual errors on these values are believed to be less than the error bars indicated.

Figures 9a and 9b confirm the general trends in recessions observed in Figs. 8a-e: recession is maximum at the stagnation point for the carbon-phenolic models and minimum for the carbon-carbon models. For carbon-carbon models, the measured recession is about 30% higher than the predicted value at the stagnation point. The difference can be attributed to spallation. For the carbon-phenolic models, the measured average recession is 62% higher than the theoretical value based on Ames conductivity and 57% higher than that based on GE conductivity. The measured char thickness at the stagnation point of the carbon-phenolic models is slightly smaller than the theoretical value.

Discussion

The depths of the indentations due to spallation are seen to be typically about 0.2 mm. Figure 2 of Ref. 1 shows the boundary layers to be about 0.8 mm thick. Therefore, the indentations probably did not alter the laminar nature of the boundary layers to a significant extent. Even if the boundary layers became turbulent, the resulting increase in convective heat-transfer rates is likely to be inconsequential in the

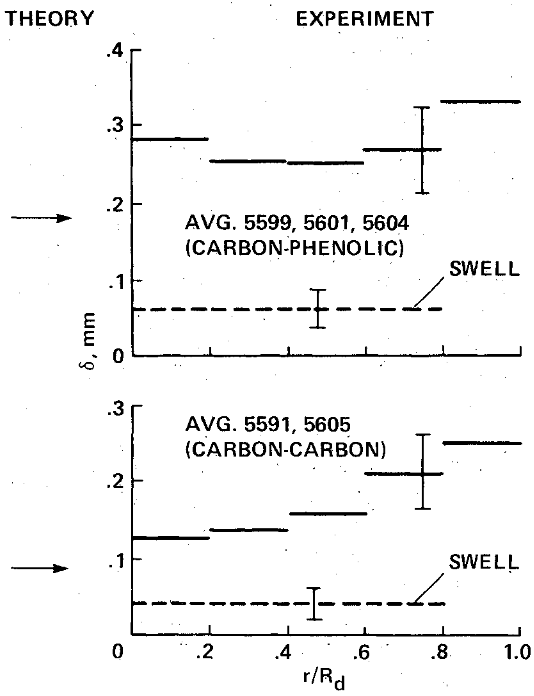

Fig. 9 Comparison of the measured and predicted average surface recessions.

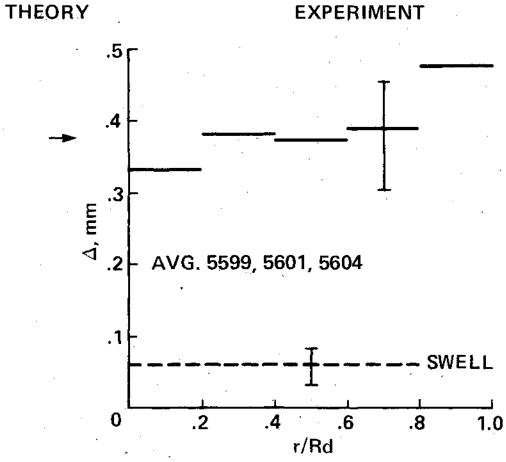

Fig. 10 Comparison of the measured and predicted average char thicknesses.

radiation-dominated, massive-blowing flowfield that prevailed in the present test environment. Ablation rate is dictated mostly by radiation, accuracy of calculation of which is verified by experiment.[2]

The difference in the recession values seen between the theory and experiment can be attributed to spallation. The evidence of spallation is seen in shadowgraphs (Fig. 2) and head-on ima-con photographs (Fig. 4). Spallation is roughly twice as severe for carbon-phenolic than for carbon-carbon. For carbon-phenolic, the extent of spallation deduced from the present experiment is higher than that observed by Lundell[10] through a laser irradiation experiment. According to the laser test data, the spallation mass-loss rate is about 18% of the thermochemical ablation rate at the heat flux of 30 kW/cm^2. In the present tests, the average wall heat flux was between 30 and 35 kW/cm^2, and spallation was about 60%. That is, the present spallation rate is nearly three times that found by the laser test. The difference may be attributed to the fact that the small particles are unaccounted for in the laser experiment: the small particles may have been oxidized to form carbon-dioxide by reacting with oxygen in air in the experiment,[10] and thereby escaped capture.

The spallation phenomenon is not accounted for in the CMA calculation used in deriving the theoretical char thicknesses: there is as yet no satisfactory theoretical model to do so. However, it is qualitatively apparent that the spallation would reduce the char thickness. A total recession of about 0.1 mm, due to spallation seen in the present experiment, is bound to cause a reduction in char thickness of a fraction of 0.1 mm. The theoretical char thickness indicated in Fig. 10 should be lowered by the corresponding amount. This will bring the theoretical char thickness value closer into agreement with the experimental data.

One interesting point to consider is the spreading of the indented areas. According to Table 1 and Fig. 6, spallation occurs randomly for the CMCP. For those models, roughly 5% of the surface areas were indented within the flight times of about 0.05 s. Therefore, the time scale of spreading of indentation is about 1 s. That is, roughly $1-1/e=0.63$ of the disk surface will be indented within 1 s. In a typical planetary entry flight, flight times extend to many seconds. For example, the heat-shield surface of the Galileo probe vehicle, which has a CMCP nose cap, will be almost totally roughened by this process during most of the flight.

From the present experiment, a rough estimate of distribution of particle sizes can be made. Figure 4a shows that the spalled particles are all very small for carbon-carbon. For carbon-phenolic, however, spalled particles range in size from very small to very large (see Fig. 4b). The shadowgraph in Fig. 2 shows only large particles, but this is probably because shadowgraph techniques cannot optically resolve small particles. The large particles must have originated in the indented sites; the indentations have typical depths of 0.2 mm and frontal diameters of up to 2 mm (see Fig. 4b), which roughly match the sizes of the observed large particles. However, the total volume of the indented sites is only about 5% of the total volume removed by ablation. Since the total mass loss that is unaccounted for is 60%, this means that only about one-tenth of the total spallation is by such large particles for carbon-phenolic.

The only substantial unexplained phenomenon concerns variations in surface recession and wall temperature with radius. Since the flow regime is radiation dominated, heat-transfer rates should be the highest at the stagnation point, where the shock layer is the hottest and the thickest, and decrease toward the edge. This expected trend is seen only in the small region ($r/R_d < 0.4$) of the carbon-phenolic models in Figs. 8 and 9. Carbon-carbon models show the opposite trend of increasing recession with radius. Even for the carbon-phenolic models, increase in wall temperature with radius seen in Fig. 5 is equally puzzling. While the model passes through helium in front of an ima-con camera, cooling by helium is at least as strong at finite radii as at the stagnation point.[9] Hence the wall temperature should appear no higher at finite radii than at the stagnation point, unless the off-stagnation point regions are initially at higher temperatures.

Since convective heat-transfer rates and surface shear forces are negligibly small in the present environment, the observed phenomena must be attributed to an increase in radiative heat-transfer rates with radius. Because there is no established theory that would explain the increase in radiation with radius one can only speculate about the cause. A possible cause for the increase is radiation of carbon species derived from the spalled particles. Davies and Park[11] show that the spalled particles travel far into the inviscid region of the shock layer. The shadowgraphs taken in the present tests, an example of which is shown in Fig. 2, also confirm this trend. According to Davies and Park, a substantial portion of the spalled particles vaporizes in the hot inviscid shock-layer region. Any gaseous carbon species released by this mechanism will quickly dissociate and ionize in the environment of the shock layer. These ionized carbon species can emit additional radiation. This aspect of the problem remains to be studied in the future.

Conclusions

The shock standoff distances, wall temperatures, and the char thicknesses for six 5-cm-diam carbonaceous disks tested in a track-range facility agree with the theoretical predictions. The surface recessions for carbon-phenolic at the stagnation point are higher than the theoretical predictions by an average of 60%. The recessions for carbon-carbon models are higher by 30%. The discrepancies between theory and experiment are attributed to spallation. Recessions increase with radii for an unknown reason.

Acknowledgments

The author wishes to express his sincere thanks to Mr. Alan M. Adams and his associates at Arnold Engineering Development Center, Arnold Air Force Station, Tennessee, for designing and fabricating the models, carrying out the tests, and reducing the basic data used in the present work.

References

[1] Park, C., "Stagnation-Point Ablation of Carbonaceous Flat Disks in an Argon-Filled Ballistic Range—Part I: Theory," *AIAA Journal,* Vol. 21. Nov. 1983, pp. 1588-1594.

[2] Park, C., "Calculation of Radiation from Argon Shock Layers," *Journal of Quantitative Spectroscopy and Radiative Transfer,* Vol. 28, No. 1, July 1982, pp. 29-40.

[3] Norfleet, G. D., Hendrix, R. E., Raper, R. M., and Callens, E. E. Jr., "Development of an Aeroballistic Range Capability for Testing Reentry Materials," *Journal of Spacecraft and Rockets,* Vol. 12, May 1975, pp. 302-307.

[4] Miller, J. T., "Aeroballistic Range Tests of Ablating Heat Shield Materials—Interim Report," Arnold Engineering Development Center, Arnold Air Force Station, Tenn., AEDC-TR-70-114, May 1970.

[5] Adams, A. M., "Hypervelocity Track Test of the Ablative Characteristics of Heat-Shield Materials for the NASA Galileo Probe," Arnold Engineering Development Center, Arnold Air Force Station, Tenn., AEDC-TSR-81-V25, Aug. 1981.

[6] Adams, A. M., "NASA/Ames Galileo Probe Heat-Shield Ablation Test 2: Data Package," Arnold Engineering Development Center, Arnold Air Force Station, Tenn., Project C378-VG-(G-15), Aug. 1981.

[7] Bueche, J. F., "Effects of Improvements and Uncertainties in Thermo-Physical Properties on Carbon-Phenolic Heat-Shield Thermal Performance Predictions," AIAA Paper 77-787, Albuquerque, N. Mex., June 1977.

[8] Wakefield, R. M. and Pitts, W. C., "Analysis of the Heat-Shield Experiment on the Pioneer-Venus Entry Probes," AIAA Paper 80-1494, Snowmass, Colo., July 1980.

[9] Kemp, N. H., Rose, P. H., and Detra, R. W., "Laminar Heat Transfer around Blunt Bodies in Dissociated Air," *Journal of the Aerospace Sciences,* Vol. 26, July 1959, pp. 421-430.

[10] Lundell, J. H., "Spallation of the Galileo Probe Heat Shield," AIAA Paper 82-0852, St. Louis, Mo., June 1982.

[11] Davies, C. B. and Park, C., "Trajectories of Solid Particles Spalled from a Carbonaceous Heat-Shield," AIAA Paper 82-0200, Orlando, Fla., Jan. 1982.